

## Statistical analysis of building-induced turbulence at an airport

K.K. HON<sup>1</sup>, Philipp LUX<sup>2</sup>, P.W. CHAN<sup>1\*</sup>, K. NGAN<sup>3</sup>, Q.S. LI<sup>3</sup> and Mark WENIG<sup>4</sup>

<sup>1</sup>*Hong Kong Observatory, 134A Nathan Road, Kowloon, Hong Kong, China.*

<sup>2</sup>*University of California, Berkeley, 101 Sproul Hall 4206, Berkeley, CA 94720-4206, USA.*

<sup>3</sup>*City University of Hong Kong, Tat Chee Avenue, Kowloon, Hong Kong, China.*

<sup>4</sup>*Ludwig-Maximilians-Universität München, Theresienstraße 39, 80333 München, Deutschland.*

\*Corresponding author: email: pwchan@hko.gov.hk1920

Received: February 25, 2020; accepted: June 25, 2020

### RESUMEN

Las turbulencias inducidas por construcciones pueden afectar la seguridad aérea, por ejemplo, cuando un avión está próximo a aterrizar en un aeropuerto. En el Aeropuerto Internacional de Hong Kong se han realizado observaciones de este tipo de turbulencia utilizando para ello un LIDAR de corto alcance (SRL, por sus siglas en inglés). En este trabajo se describe el análisis estadístico de la velocidad radial, en particular de la función de la estructura longitudinal. Se ha encontrado que la teoría clásica sobre turbulencia homogénea de Kolmogorov puede aplicarse a las observaciones con LIDAR de flujos de aire perturbados por construcciones. También se analizan algunas características distintivas de los flujos turbulentos, en especial las rachas de velocidad y pequeños anticiclones en escala de hectómetros. Se examina el impacto potencial en un avión en aterrizaje y se compara con la información de vuelo. Los resultados del presente estudio pueden ser de utilidad para estudiar turbulencias inducidas por construcciones en otros aeropuertos del mundo.

### ABSTRACT

Building-induced turbulence may affect aviation safety, e.g., when the aircraft is about to land at an airport. Observations of such flow have been conducted at the Hong Kong International Airport using short-range LIDAR (SRL). Statistical analysis of the radial velocity, namely, the longitudinal structure function, is described herein. It is found that the classical Kolmogorov theory for homogeneous turbulence applies to LIDAR observations of building-disrupted airflow. Some distinctive features of the turbulent flow are also discussed, notably velocity streaks and tiny anticyclones at the hectometer scale. The potential impact on a landing aircraft is examined and compared to flight data. The results in this paper could be useful for studying building-induced turbulence at other airports around the world.

**Keywords:** LIDAR, building effect on the wind, longitudinal structure function.

### 1. Introduction

The Hong Kong International Airport (HKIA) is in an area of complex terrain. It is surrounded by seas to three sides and the mountainous Lantau Island to the south. Low-level windshear and turbulence have been observed to arise from the terrain-disrupted airflow (e.g., Shun et al., 2003; Shun and Chan,

2008). HKIA is also located in a densely built-up area as many engineering and commercial services are connected to the airport. Low-level building-induced turbulence, e.g., near aircraft touchdown, has been reported by Chan and Krus (2016) and Chen et al. (2019). However, direct observation of building-induced airflow disturbances has been rather rare

because their spatial and temporal scales are small compared to their terrain-induced counterparts.

Low-level windshear and turbulence arising from man-made structures have been reported in other airports, such as Schiphol in the Netherlands. Comprehensive review of such turbulent flows can be found in Krüs (2016) and Krüs et al. (2003). Nieuwpoort et al. (2006) conducted a very detailed study of the turbulent airflow that has also formed the basis of the alerting criteria (also known as seven-knot criteria) for building-induced turbulence. It is a pioneering work, whose criteria has been adopted in the assessment of building-induced turbulence in Hong Kong.

In order to observe and provide advanced warning of building-induced turbulence at HKIA, a permanent short-range LIDAR (SRL) unit was installed by the Hong Kong Observatory (HKO). A seaside site at the northeastern corner of the airport island, next to a convention center, namely, the AsiaWorld-Expo (Fig. 1) was chosen because many pilot reports indicate disrupted airflow in its vicinity when aircrafts

arrive at the northern runway of HKIA from the east. This runway, referred to as 25RA, is shown in Figure 2. AsiaWorld-Expo has a height of about 25 m, which is comparable to the aircraft elevation shortly before touchdown at 25RA.

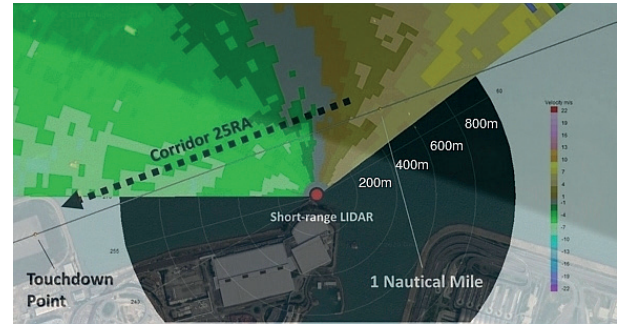


Fig. 2. Diagram showing the geometry of the SRL scanning.

The statistics of low-level wind shear over 25RA before the construction of AsiaWorld-Expo (around 2004) and after the building was in place have been analyzed. Only the windshear reports for background south to southwesterly winds and reported heights at 300 m or less have been calculated. The windshear frequency has been calculated by normalizing the total number of windshear reports under the above-described conditions with the number of flights over 25RA. The windshear frequency increased from about 0.11 to 0.19% before the construction of AsiaWorld-Expo to 0.19 to 0.37% after its construction. This is consistent with pilot observations that low level windshear appears to have increased after the construction of the building.

The use of SRL at HKIA has been reported in a number of previous field campaigns, e.g., Chan and Lee (2012), Hon et al. (2014), and Hon and Chan (2017). SRL has several advantages over long-range LIDAR, which is effective for alerting terrain-induced airflow disturbances. These include fine radial resolution (about 30 m) and high temporal resolution (scanning every 20 s), though the measurement range is limited to a maximum of only 3–6 km, depending on the weather conditions and instrument configuration. These advantages make SRL a suitable tool for observing the rapidly evolving, and fine-scale airflow disturbances induced by the buildings.



Fig. 1. (a) Overview of HKIA and its buildings; (b) diagram specifically showing the AsiaWorld-Expo (red square) and the SRL (orange dot).

Compared with previous SRL studies, this paper has two novel aspects. First, a statistical analysis of airflow disturbances over 25RA is performed for two distinct wind directions: easterly flow, which is relatively free from localized disruption by buildings (the main source of disruption being the Lantau terrain); and southerly flow, which is much disrupted by the Lantau terrain and the building cluster immediately upstream of 25RA (i.e., AsiaWorld-Expo and its neighbors). To the knowledge of the authors, this is the first time that statistical analysis is conducted for Doppler LIDAR measurements for both terrain and building-induced airflow disturbances at a spatial resolution below 100 m. Second, direct observations of building-induced turbulence by SRL are reported, including velocity streaks in a typhoon situation and microscale anticyclones. In the latter case, an analysis of corresponding flight data from the aircraft, including a pilot report of unstable aircraft operation, is conducted for the first time.

## 2. Instrumentation

The SRL is a coherent Doppler LIDAR of the Streamline model manufactured by Halo Photonics. It operates at a wavelength of 1.5  $\mu\text{m}$  in the infrared spectrum and possesses eye-safe Class 1M power. The maximum unambiguous radial velocity is  $\pm 19 \text{ ms}^{-1}$ . The size of each range gate is 30 m. The SRL is configured to perform surveillance over the final stretch of corridor 25RA in a manner similar to previous field campaigns conducted by HKO (Chan and Lee, 2012; Hon et al., 2014). The scanning strategy is based on fast plan position indicator (PPI) scans at constant elevation angle of  $3^\circ$  covering the northern sector with azimuthal angles between  $270^\circ$  and  $50^\circ$ , so that the scanning area covers part of the 25RA landing path. Each one-way scan (i.e., from  $270^\circ$  across  $0^\circ$  to  $50^\circ$ , or the other way around) takes about 20 s to complete, and the cycle is repeated continuously. Scan data from both directions are used and processed in an identical manner.

## 3. Statistical analysis of Doppler velocity from LIDAR

The Kolmogorov theory of homogeneous and isotropic turbulence (e.g., Pope, 2000) is the basis for

understanding turbulent flows. Specific predictions of the theory have been verified for many experimental and numerical configurations. Applicability to turbulent flow around the HKIA is uncertain because, strictly speaking, the presence of mountains or buildings violates the assumption of homogeneity.

A well-known prediction of the Kolmogorov theory concerns the second-order velocity structure function, which is the covariance of the velocity difference between the positions  $\vec{x}$  and  $\vec{x} + \vec{r}$ :

$$D_{ij}(\vec{r}, \vec{x}, t) \equiv \langle [\vec{U}_i(\vec{x}, \vec{r}, t) - \vec{U}_i(\vec{x}, t)] [\vec{U}_j(\vec{x}, \vec{r}, t) - \vec{U}_j(\vec{x}, t)] \rangle \quad (1)$$

The normalized longitudinal structure function satisfies

$$\frac{D_{11}}{(\varepsilon r)^{2/3}} = C_2 \quad (2)$$

where  $\varepsilon$  is the energy dissipation rate,  $C_2$  is a constant and the index '1' denotes the along-wind or longitudinal direction. Kolmogorov theory predicts that the normalized second-order structure function is constant within the inertial range. More generally, the scaling of higher-order structure functions depends on  $p$ , the order of the structure function (Frisch, 1995).

The LIDAR beam at a specific azimuth and time measures the radial wind velocity at a known separation from the SLR. There are 100 points (separated by 30 m) along the beam, yielding a total range of 3000 m. The time dependence is neglected as the measurements are considered to be instantaneous. Thus, the longitudinal direction (i.e., direction 1 in Eq. [2] above) is assumed to be the radial direction of the laser beam. The usable distances  $r$  are limited by the range gate length of 30 m. For each value of  $r$ ,  $D_{11}$  is taken to be the mean of the squares of all the velocity differences. The Kolmogorov prediction applies where  $D_{11}/r^{2/3}$  is approximately independent of  $r$ . Although  $\varepsilon$  could be estimated using standard algorithms (e.g., Chan, 2011; Frehlich et al., 2001), this is not required to diagnose an inertial range.

In the present calculation, days with southerly and easterly winds are analyzed. Data covers all of 2018. The easterly winds are oriented mainly from the sea towards the HKIA and experience a relatively small degree of terrain disruption (by the terrain of eastern Lantau Island only). By contrast, the

southerly wind is mainly disrupted by the buildings on the airport island immediately upstream of the SRL. Radial beams with directions of  $80^\circ$  to  $100^\circ$  are considered for easterly winds, while beams of  $350^\circ$  to  $10^\circ$  are considered for southerly winds. The mean wind speed for each case is at least  $5 \text{ ms}^{-1}$ . The data (output from the manufacturer's software) are also filtered according to the signal-to-noise ratio (SNR). For this calculation, only data with a  $\text{SNR} > 1.05$  are considered. The number distribution of the measurements is shown in Figure 3a. After filtering for time, direction, speed and SNR, each measurement within 1 h is used to calculate the second-order structure function. Taking the mean of these structure functions yields the time-averaged structure function for the hour in question. Averaging over the hourly structure functions gives the structure function for easterly or southerly winds.

The structure function  $D_{11}$  is plotted in Figure 3b for southerly and easterly flows. There is an approximately monotonic, increasing trend in the latter case. In Figure 3c, the normalized structure function,  $D_{11}/r^{2/3}$ , is plotted against  $r$ . Deviations from a constant horizontal line are indicative of the breakdown of the Kolmogorov theory. It can be seen that the normalized structure function is nearly constant up to about  $r \approx 1400 \text{ m}$  for southerly winds and  $r \approx 500 \text{ m}$  for easterly winds. The results within these subranges are consistent with the Kolmogorov theory. Since the breakdown occurs at relatively large scales, it may be ascribed to meteorological influences.

#### 4. Tropical cyclone case

The case occurred on August 27, 2017 when Hong Kong was affected by the severe tropical storm Pakhar. In the morning of that day, Pakhar was located around 100–50 km to the southwest of Hong Kong (Fig. 4a) and brought storm-force winds to the HKIA region. From Figure 4b it can be seen that the region of 25RA (one nautical mile [NM] from the runway threshold to touchdown) experienced a wind speed of 30 to 35 kt. The south-southeasterly winds crossed over the buildings at the northeastern corner of HKIA island and airflow disturbances can be expected over 25RA. The atmospheric stability in the morning of that day, namely 00:00 UTC (Hong Kong time = UTC + 8 h) is shown in the tephigram

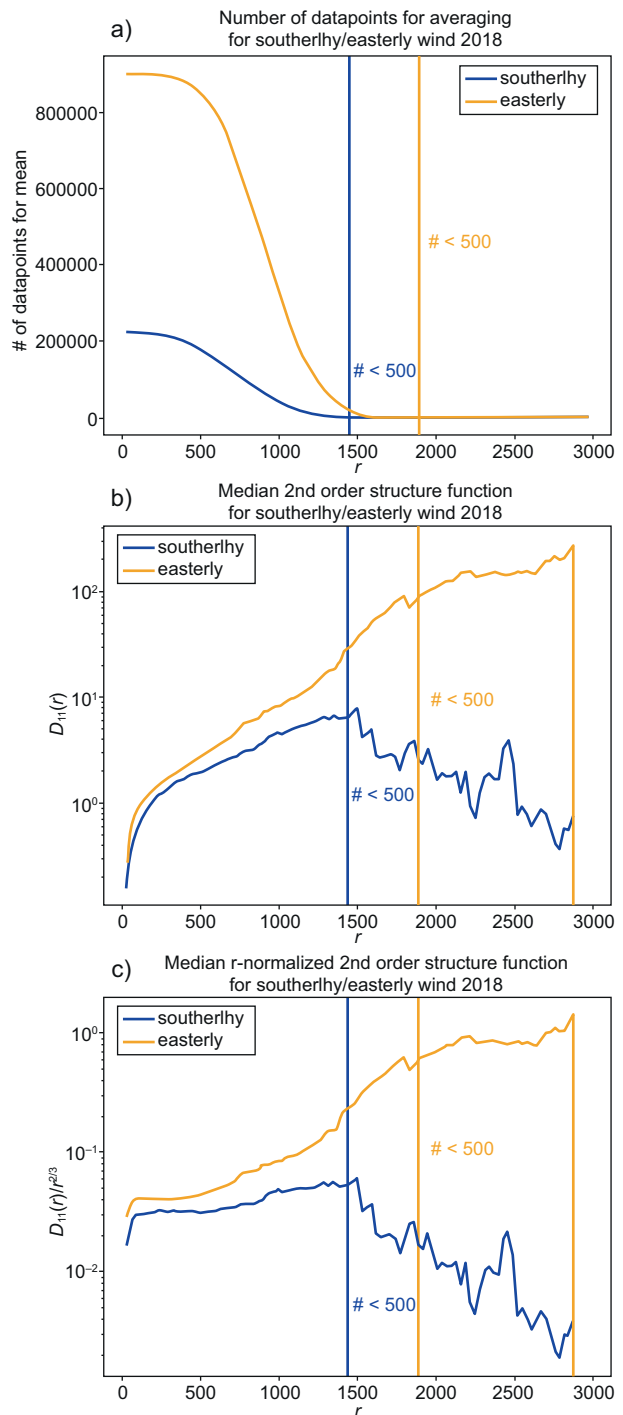


Fig. 3. Second-order structure function calculation. (a) Number of datapoints used for the averaging procedure over  $r$ . (b) Southerly and easterly structure functions plotted over  $r$ . Vertical lines show the threshold of 500 used datapoints. (c) Normalized southerly and easterly structure functions plotted over  $r$ . Vertical lines show the threshold of 500 used datapoints.

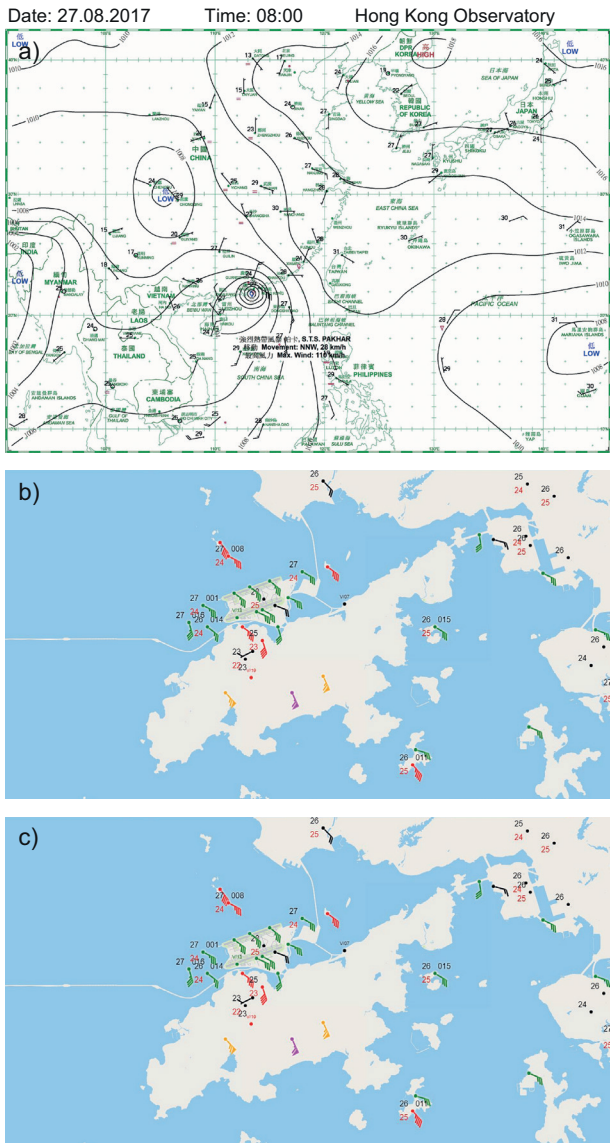


Fig. 4. Meteorological data for the tropical cyclone case on August 27, 2017. (a) Synoptic surface weather chart at 08:00 LT; (b) surface observations at 09:30 LT; (c) tephigram at 00:00 UTC.

(Fig. 4c) based on the radiosonde launched at King's Park of Hong Kong (about 20 km to the east of HKIA over the city center). The lower troposphere is saturated and follows the saturated adiabatic lapse rate.

Figure 5 shows some typical examples of Doppler velocity observations by the SRL from that morning. Due to the rather moist atmosphere, the measurement range of SRL was limited to the first

couple of kilometers from the LIDAR. Nevertheless, a number of velocity streaks were clearly observed by the SRL. The velocity is so high that folding of the radial velocity can be seen. Taking the folding into consideration, the maximum Doppler velocity is about  $25 \text{ ms}^{-1}$ .

Velocity streaks have been reported previously at HKIA (e.g., Shun and Chan, 2008) as a result of the terrain-disrupted airflow. They have also been reported in the boundary layer flow of typhoons (e.g., Shun et al., 2003). However, the streaks are thinner and more closely packed in the present case. They are believed to arise from the buildings, maybe together with hectometer-scale boundary layer rolls in the typhoon (e.g., Li and Chan, 2012; Li et al., 2019). From Figure 5 there could be three to four velocity streaks appearing in the rather limited azimuthal coverage of the LIDAR. There was no aircraft operation at the time of the tropical cyclone passage. If there had been an aircraft moving along 25RA by that time, it would have experienced velocity rise and fall when crossing the streaks. The SRL can capture and possibly provide timely alerts to the aircraft arising from such airflow disturbances. This points to the importance of the SRL in aviation meteorological applications.

The velocity streaks could lead to turbulent airflow being encountered by the arriving aircraft. As it flies through the higher velocity streaks and lower velocity areas in between, the changing crosswind could be felt as turbulence. Also, the locations of higher velocity streaks and lower velocity areas could change with time. This complicates the turbulence to be felt by the aircraft.

## 5. Microscale anticyclone leading to flight instability

Around noon on August 13, 2017, a moderate southwesterly flow associated with the southwest monsoon was affecting the southern coast of China (Fig. 6a). The winds over 25RA were not strong (Fig. 6b). The winds over the northern runway of HKIA were generally in the southwest direction, where the 1 NM area had a weak south-southwesterly flow. From Figure 6c, the lower troposphere (approximately 1 km above the mean sea level) follows the dry adiabatic lapse rate. No temperature inversion nor isothermal layer were observed over that altitude range. Under such condition,

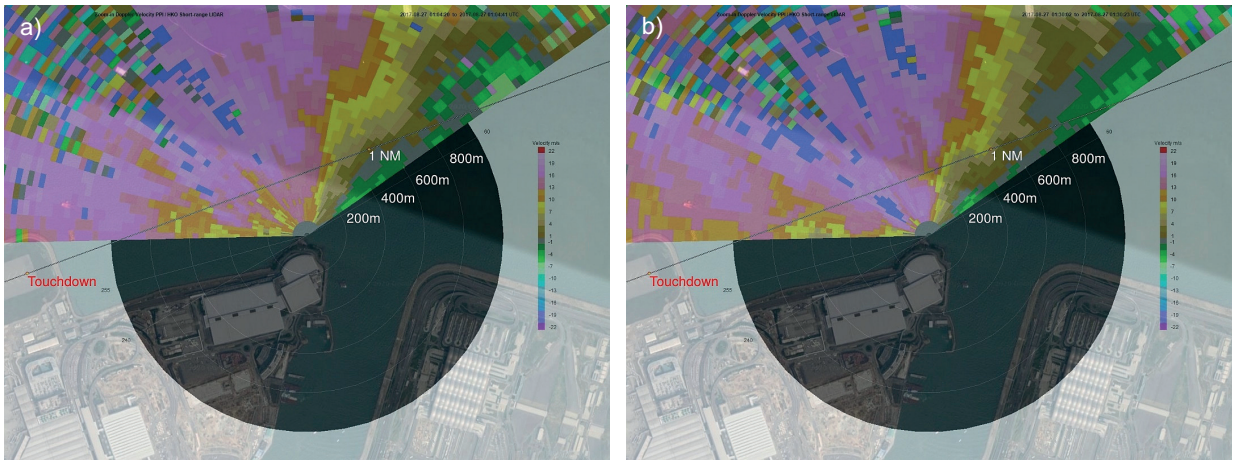


Fig. 5. Velocity streaks in the tropical cyclone case. Streaks are highlighted in dark blue and the folding of radial velocity is represented with a cool color within the warm color. (a) and (b) show examples of the streaks at two difference time instances.

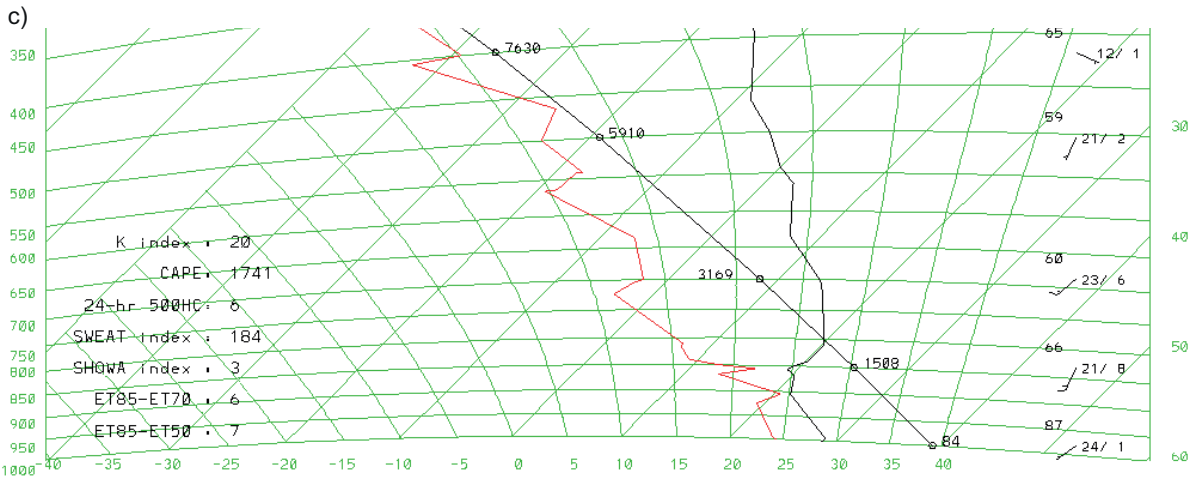
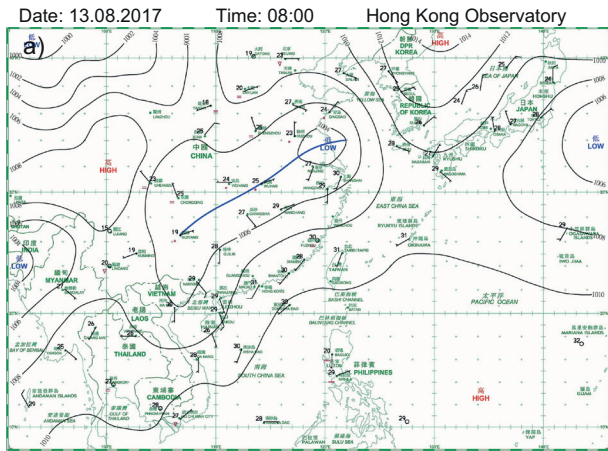


Fig. 6. Same as Figure 4, but for a southerly wind case.

the weather appears to be so benign that no low-level windshear or turbulence could be expected.

However, under the background moderate southwesterly flow, an airflow disturbance has been observed by the SRL. The sequence of SRL velocity imagery is shown in Figure 7. It could be that a tiny anticyclone, extending only over a distance of about 500 m, occurred to the immediate west of the SRL and drifted to the east-northeast along the extended center of the runway following the background southwesterly flow. The anticyclone appeared to grow in intensity during the evolution, from about  $4 \text{ ms}^{-1}$  outbound flow at first, to about  $10 \text{ ms}^{-1}$  outbound flow later. The size of the anticyclone was also growing.

To our knowledge, no such microscale anticyclone observed by a LIDAR has been reported before. In

view of the rapid development of the anticyclone and its rather limited size, it is believed to arise from both the building-induced turbulence and the effect of the Lantau terrain on the rather moderate southwesterly flow.

Possibly as a result of such an airflow disturbance, an aircraft reported instability in operation when touching down at the northern runway of HKIA in the 25RA runway corridor. The report by the pilot is the following:

“I have just had another incident today with the first officer flying the aircraft, this time a 777-200. The atis as I recall was giving the wind at ABOUT 210/8, the preceding a/c was given a landing wind of 250/8, the preceding a/c was given a landing wind of 250/8, our landing wind was given as ABOUT 220/230 at 9 kts so we were not expecting any wind shift. I was watching the wind on the aircraft’s

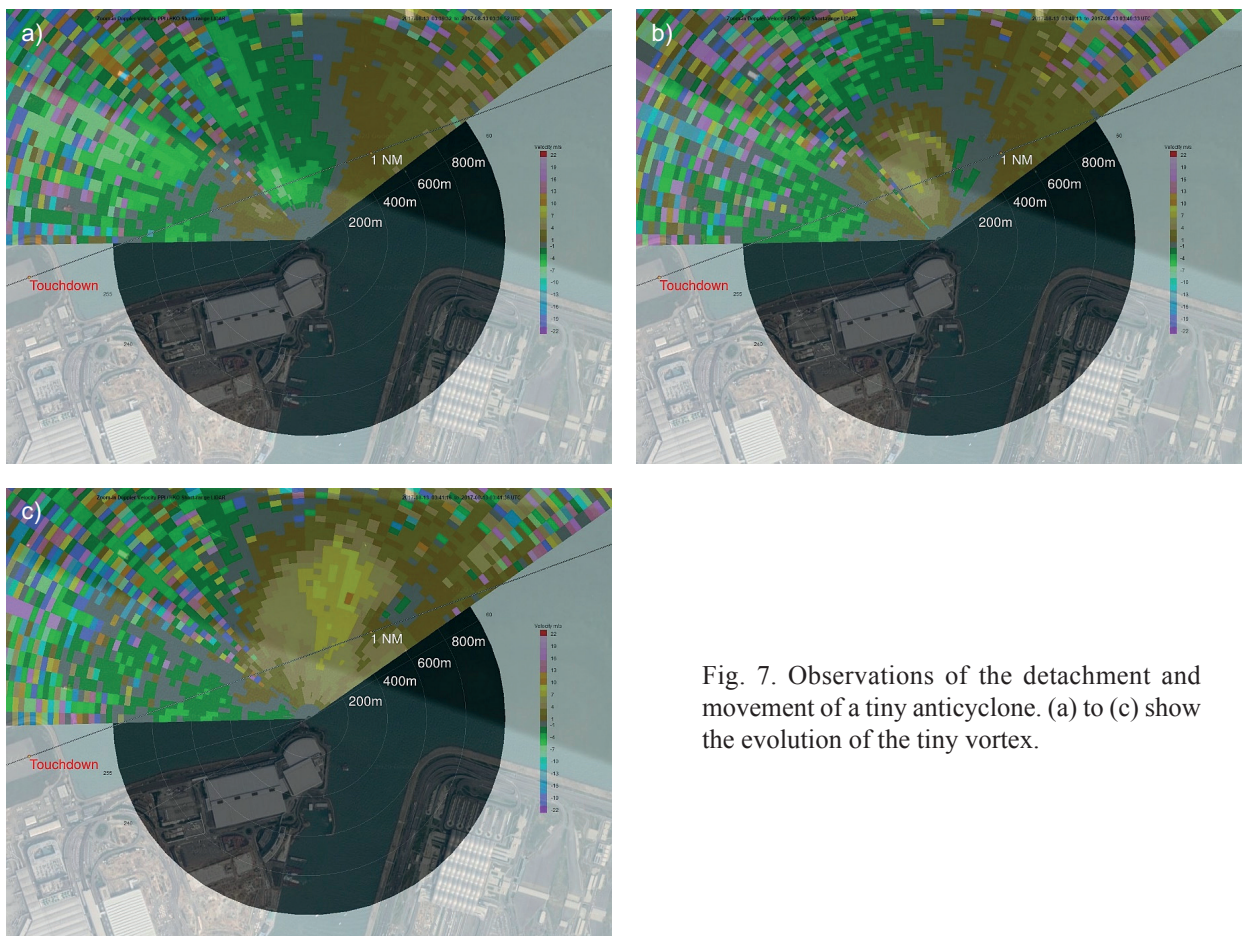


Fig. 7. Observations of the detachment and movement of a tiny anticyclone. (a) to (c) show the evolution of the tiny vortex.

instruments and vaguely remember thinking the wind had backed a little suggesting something like 210/8. At 100 ft the aircraft banked some 10-15° to the right and the speed dropped by 5 kts. At about 200 ft previously we had rising wind shear, nothing violent but definitely noticeable. The first officer brought the wing back up as he was manually flying the a/c and the auto throttle added some power to regain the speed. At 50 ft we had one dot fly up on the ils and three reds on the papi's. We reported this to atc who advised the following a/c.”

The aircraft data of that flight was obtained and the key parameters are plotted in Figure 8. The headwind measured on the aircraft changed from 3 to about 15 kt (Fig. 8a). The magnitude of the headwind change does not yet correspond to a

significant windshear. From Figure 8b, the eddy dissipation rate (EDR, see Haverdings and Chan, 2010) is about  $0.3 \text{ m}^{2/3}\text{s}^{-1}$  at about touchdown. This is a case of moderate turbulence. The roll angle (Fig. 8c) is about  $\pm 5^\circ$  below 1 nm. This is smaller than the pilot's descriptions. At some point the descent rate (Fig. 8d) reached  $-1200 \text{ ft m}^{-1}$ , which is considered to be very significant (e.g., Chan and Krus, 2016). Based on the flight data, it is a case of low-level moderate turbulence. The roll angle and descent rate are rather large. This is consistent with previous simulation studies (e.g., Chan and Krus, 2016) where the building-induced turbulence may result in a roll angle of  $4^\circ$  to  $7^\circ$  and a descent rate of 900 to  $1000 \text{ ft m}^{-1}$  for the buildings at the northeastern part of HKIA. The SRL provides very useful data

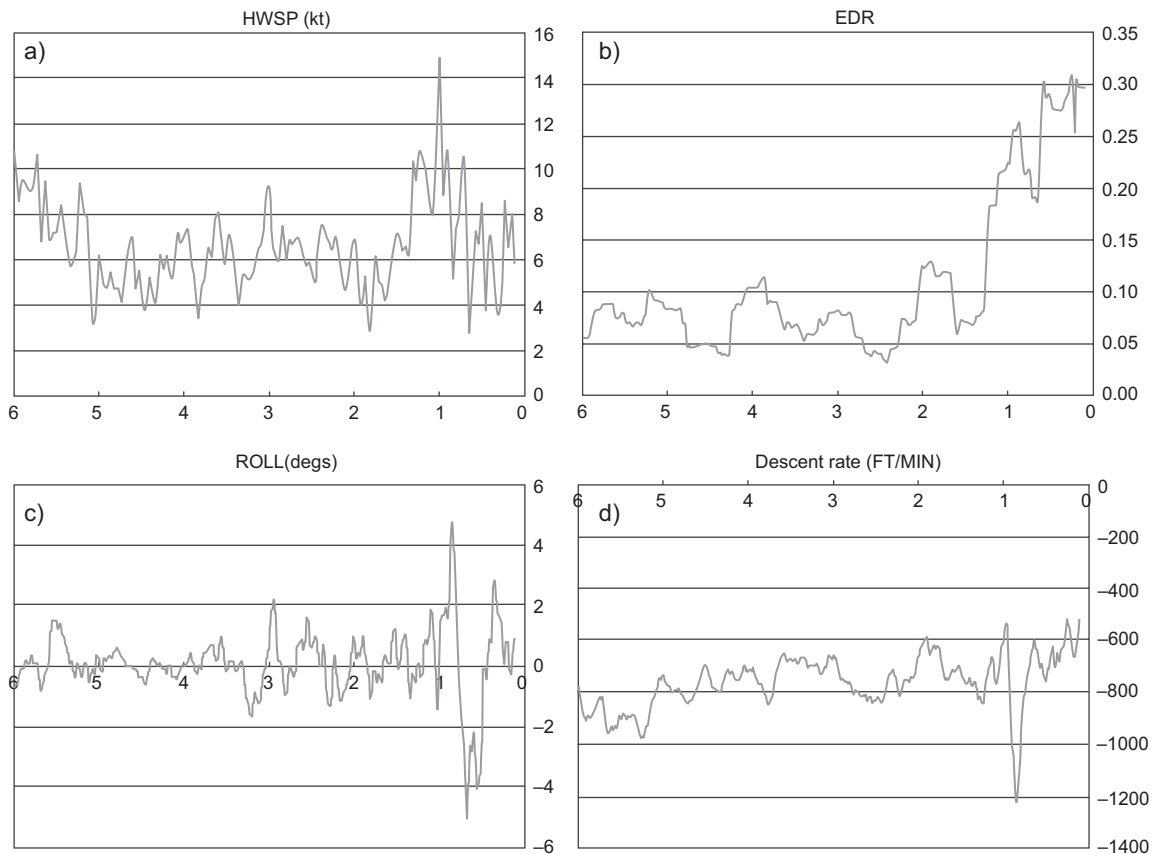


Fig. 8. Data of a landing aircraft experiencing building-induced turbulent. The  $x$ -axis is the distance in nautical miles from the eastern threshold of the north runway (from 6 NM to touchdown). (a) Headwind speed in knots. (b) Eddy dissipation rate (EDR). (c) Roll angle (in degrees) of the aircraft. (d) Descent rate ( $\text{ft min}^{-1}$ ) of the landing aircraft.

for capturing and possibly alerting the occurrence of airflow disturbances.

**6. Multiple occurrences of microscale anticyclones**

In the above-mentioned case, the microscale anticyclone appeared just once. There could be situations with multiple occurrences of tiny anticyclones, one of which occurred on the afternoon of July 25, 2019. From the synoptic pattern shown in Figure 9a, the south to southwesterly flow was prevailing over south China coast. Similar to the above-mentioned case, south to southwesterly surface winds were reported over the 25RA runway corridor (Fig. 9b). Wind speed and direction at the eastern end of northern runway as well as the location of about 1 NM to the east of the runway threshold are quite similar to the previous

case. Moreover, the atmosphere up to about 1 km or so above mean sea level follows the dry adiabatic lapse rate.

A number of tiny anticyclones were observed by the SRL for this case. They have a lifetime of a couple of minutes within the coverage of the LIDAR. Some examples are shown in Figures 10 to 12. There are a number of observations:

- a. All the tiny anticyclones appear to the west of the SRL and move to the northeast following the background flow. However, their locations of first appearance could be quite different. There does not seem to be a “preferred” or favorable location for the generation of these tiny cyclones.
- b. Some tiny anticyclones grow in intensity when they evolve, based on the magnitude of the outbound flow (Figs. 11 and 12). However, the

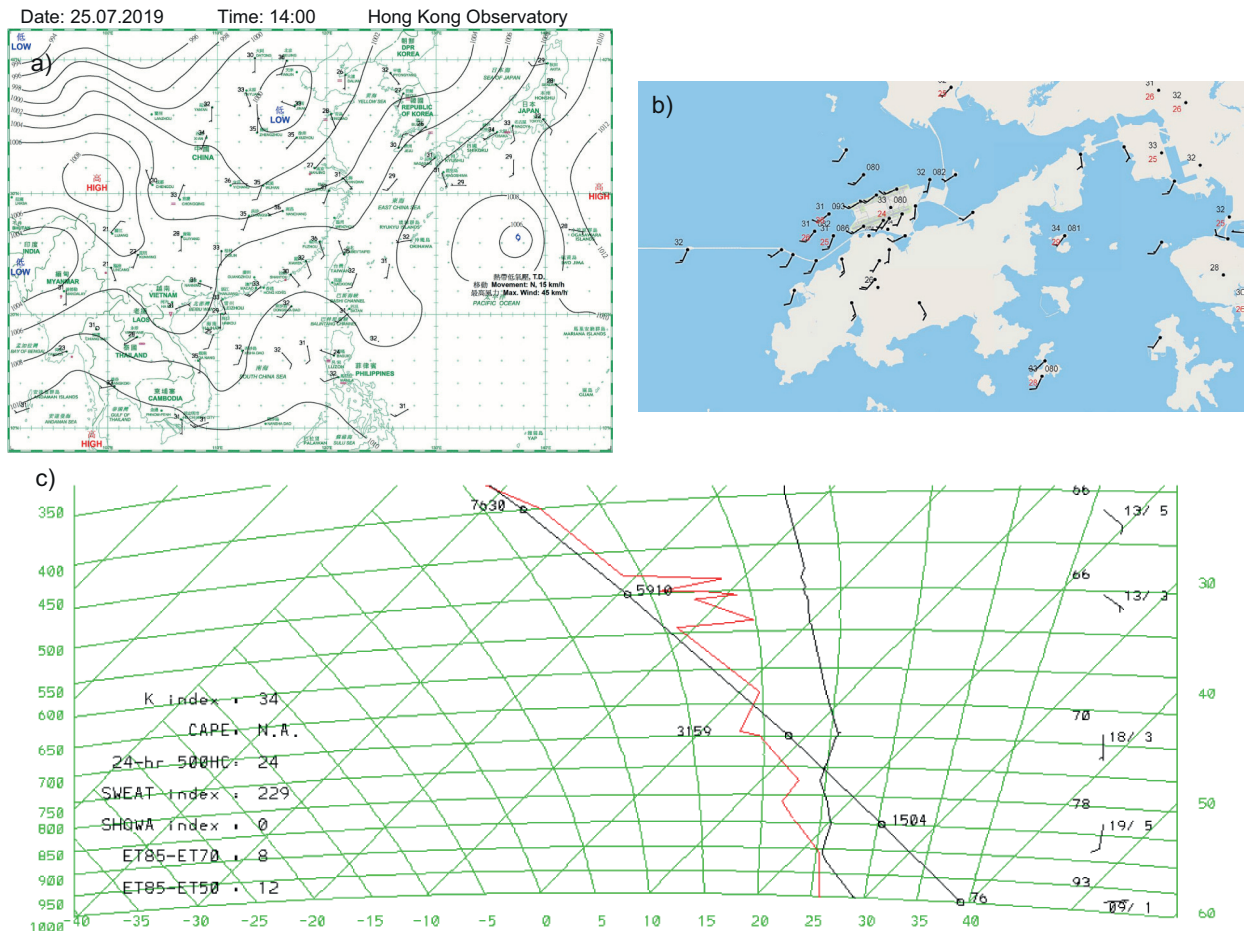


Fig. 9. Same as Figure 4, but for another southerly wind case in July 2019.

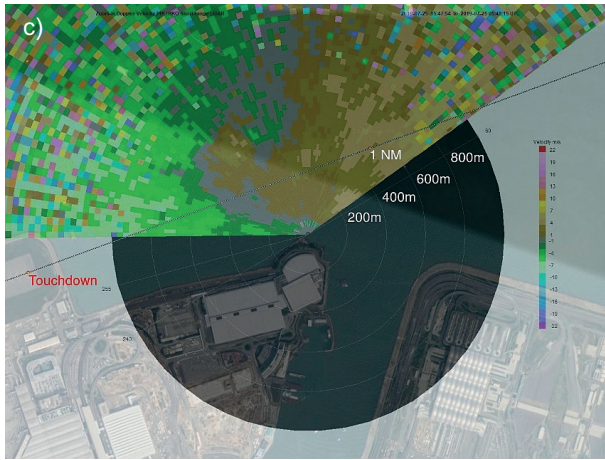
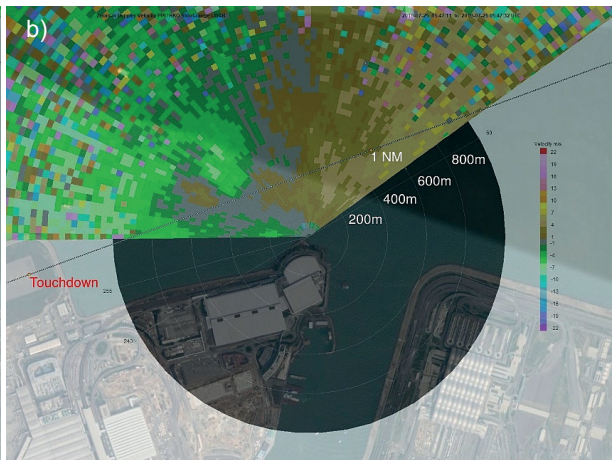
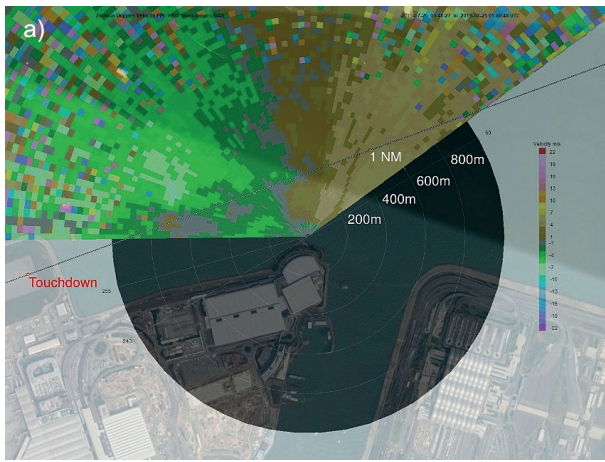


Fig. 10. Time sequence of the detachment and evolution of a tiny anticyclone. (a) to (c) show the evolution of the tiny vortex.

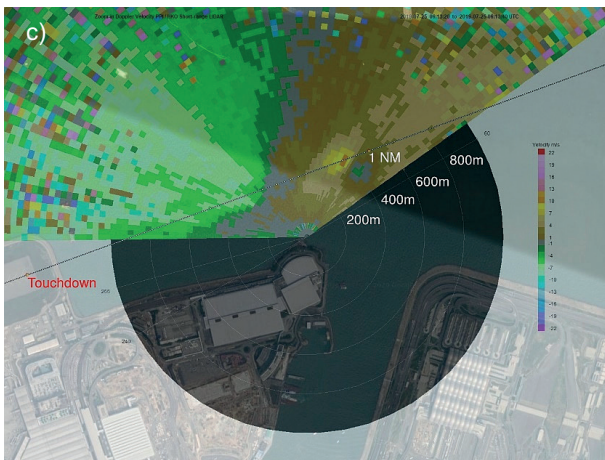
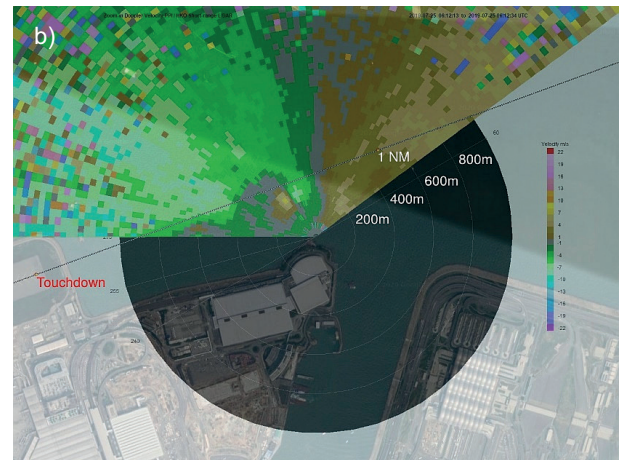
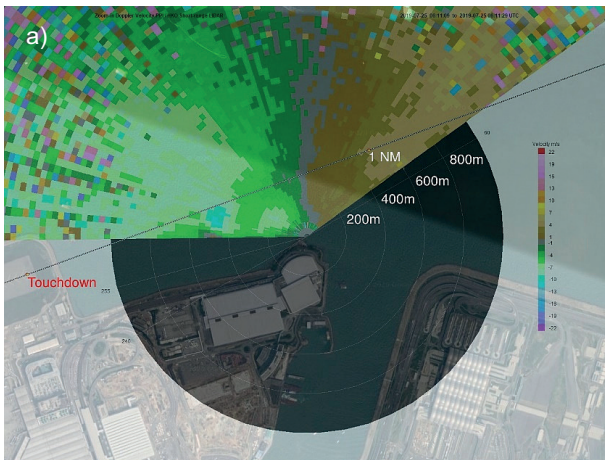


Fig. 11. Same as Figure 10, but for another case. (a) to (c) show the time evolution.

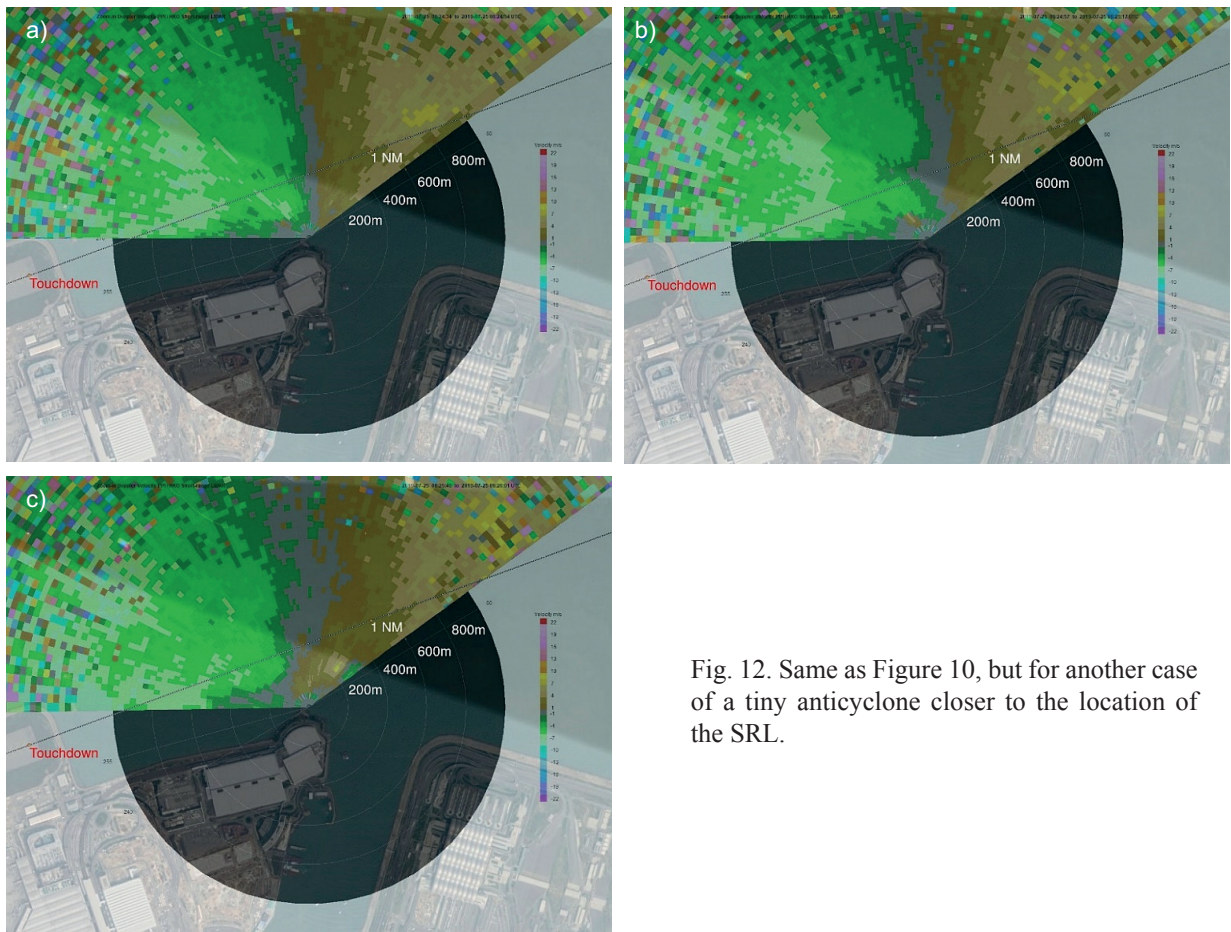


Fig. 12. Same as Figure 10, but for another case of a tiny anticyclone closer to the location of the SRL.

anticyclone may remain weak throughout the lifespan (Fig. 10).

- c. The tiny anticyclones could be of different size. For instance, the case of Figure 12 was chosen because it was rather small in size throughout its lifetime.

## 7. Conclusions

Statistical analysis of building-induced airflow was documented in this paper. For the southerly flow, the second-order longitudinal structure function is consistent with the classical Kolmogorov theory for homogeneous and isotropic turbulence. However, the width of the effective inertial range depends on the wind direction and the local contribution from inhomogeneous building-induced turbulence. This also shows that the SRL provides high-quality data for the observation and analysis of turbulence

arising from building-disturbed flows along the 25RA runway corridor.

Some examples of building-induced turbulent flows were presented. There can be streaks in the velocity imagery, arising from nearby buildings rather than the terrain. Tiny anticyclones are a common feature in the moderate southwest monsoon. Some characteristics of such cyclones were also discussed. The SRL has a good performance in capturing and possibly alerting of such airflow disturbances. It is found that, in meteorologically benign days, there could be airflow disturbances affecting flight stability and safety.

The origin of such building-induced turbulence requires further study. It is still not possible to forecast in advance which days are most favorable to the occurrence of such disturbances. This is because the generation mechanism of tiny anticyclones is not well known. The authors are carrying on computer simulations to see if the disturbances can be reproduced.

If useful results are obtained, they could be reported in future papers.

## References

- Chan PW. 2011. Generation of an eddy dissipation rate map at the Hong Kong International Airport based on Doppler Lidar data. *Journal of Atmospheric and Oceanic Technology* 28: 37-49. <https://doi.org/10.1175/2010JTECHA1458.1>
- Chan PW, Lee YF. 2012. Application of short-range Lidar in wind shear alerting. *Journal of Atmospheric and Oceanic Technology* 29: 207-220. <https://doi.org/10.1175/JTECH-D-11-00086.1>
- Chan PW, Krus H. 2016. Validation of a crosswind change criterion for building induced airflow disturbances using a flight simulator: Case studies at the Hong Kong International Airport. *Meteorological Applications* 23: 742-748. <https://doi.org/10.1002/met.1598>
- Chen F, Peng H, Chan PW, Zeng X. 2019. Low-level wind effects on the glide paths of the North Runway of HKIA: A wind tunnel study. *Building and Environment* 164: 106337 <https://doi.org/10.1016/j.buildenv.2019.106337>
- Frehlich R, Cornman L, Sharman R. 2001. Simulation of three-dimensional turbulent velocity fields. *Journal of Applied Meteorology* 40: 246-258. [https://doi.org/10.1175/1520-0450\(2001\)040<0246:SOTDTV>2.0.CO;2](https://doi.org/10.1175/1520-0450(2001)040<0246:SOTDTV>2.0.CO;2)
- Frisch U. 1995. *Turbulence: The legacy of A.N. Kolmogorov*. Cambridge University Press.
- Krüs HW, Haanstra JO, van der Ham R, Schreur B, Wichers. 2003. Numerical simulations of wind measurements at Amsterdam Airport Schiphol. *Journal of Wind Engineering and Industrial Aerodynamics* 91: 1215-1223. [https://doi.org/10.1016/S0167-6105\(03\)00079-5](https://doi.org/10.1016/S0167-6105(03)00079-5)
- Krüs HW. 2016. Criteria for crosswind variations during approach and touchdown at airports. *Advances in Simulation of Wing and Nacelle Stall* 131: 167-187. [https://doi.org/10.1007/978-3-319-21127-5\\_10](https://doi.org/10.1007/978-3-319-21127-5_10)
- Haverdings H, Chan PW. 2010. Quick Access Recorder (QAR) data analysis software for studies of wind-shear, turbulence and wake vortex. *Journal of Aircraft* 47(4):1443-1447. <https://doi.org/10.2514/1.46954>
- Hon KK, Chan PW, Chiu YY, Tang W. 2014. Application of short-range LIDAR in early alerting for low-Level windshear and turbulence at Hong Kong International Airport. *Advances in Meteorology* 2014: 162748. <https://doi.org/10.1155/2014/162748>
- Hon KK, Chan PW. 2017. Aircraft wake vortex observations in Hong Kong. *Journal of Radars* 2017: 709-718. <https://doi.org/10.12000/JR17072>
- Li L, Chan PW. 2012. Numerical simulation study of the effect of buildings and complex terrain on the low-level winds at an airport in typhoon situation. *Meteorologische Zeitschrift*, 21: 183-192. <https://doi.org/10.1127/0941-2948/2012/0252>
- Li L, Kareem A, Hunt J, Feng, Chan PW, Xiao Y, Li C. 2019. Observed sub-hectometer-scale low level jets in surface-layer velocity profiles of landfalling typhoons. *Journal of Wind Engineering and Industrial Aerodynamics* 190: 151-165. <https://doi.org/10.1016/j.jweia.2019.04.016>
- Nieuwpoort AMH, Gooden JMH, de Prins JL. 2006. Wind criteria due to obstacles at and around airports. Technical Report NLR-CR-2006-261. Nationaal Lucht-en Ruimtevaart Laboratorium, The Netherlands.
- Pope SB. 2000. *Turbulent Flows*, Cambridge University Press. Available at: <https://www.cambridge.org/core/books/turbulent-flows/C58EFF59AF9B81AE-6CFAC9ED16486B3A>
- Shun CM, Lau SY, Lee O. 2003. Terminal Doppler Weather Radar observation of atmospheric flow over complex terrain during tropical cyclone passages. *Journal of Applied Meteorology* 42: 1697-1710. [https://doi.org/10.1175/1520-0450\(2003\)042<1697:T-DWROO>2.0.CO;2](https://doi.org/10.1175/1520-0450(2003)042<1697:T-DWROO>2.0.CO;2)
- Shun CM, Chan PW. 2008. Applications of an infrared Doppler Lidar in detection of wind shear. *Journal of Atmospheric and Oceanic Technology* 25: 637-655. <https://doi.org/10.1175/2007JTECHA1057.1>